Film condensation on a vertical sinusoidal fluted tube

V. K. Garg*
Department of Mechanical Engineering, Indian Institute of Technology, Kanpur, India

P. J. Marto
Department of Mechanical Engineering, Naval Postgraduate School, Monterey, CA 93943, USA

Received 4 September 1986 and accepted for publication 3 August 1987

An analysis of laminar film condensation on a vertical fluted tube has been made considering gravitational and surface tension effects over the entire fluted surface, and using surface-oriented coordinates. For the first time surface tension effects are determined, as they should be, from the shape of the condensate-vapor interface rather than from the shape of the flute. Two-dimensional conduction within the condensate film as well as in the fluted tube wall is considered. A finite difference solution of the highly nonlinear partial differential equation for the film thickness is coupled with a finite element solution of the conduction problem. The procedure has been tested on a sinusoidal flute with amplitude-to-pitch ratio ~0.2. A linear extrapolation on a log-log basis of the results shows good agreement with experiment data.

Keywords: condensation; fluted tube; heat

Introduction

Many methods[1] for enhancing condensation heat transfer have been proposed. Among them, Gregorig[2] first recognized the importance of surface tension in film condensation on vertical fluted tubes such as the one shown in Figure 1. Thereafter, many experimental studies[3-9] on vertical fluted surfaces were made to confirm his findings. They all found about four to eight times larger heat transfer coefficients than those on a vertical smooth tube. Gregorig's theoretical model has also been improved upon, but much still remains to be done. Edwards *et al.*[10] proposed a condensation model on a heat transfer surface of triangular fins with the assumption that the liquid film was attached to the tip of the fin with a finite contact angle. The effect of a locally thin condensate film on the side of the fin was not considered by them, nor by Fujii and Honda[11]. Mori *et al.*[12] considered the effect of a thin condensate film on the side of the fin but neglected the variation of its thickness in the vertical direction. Hirasawa *et al.*[13] improved upon Ref. 12 in that they included the variation of a thin condensate film in the vertical direction, but they completely neglected conduction within the fin and the film. Panchal and Bell[14,15] also neglected conduction within the fin and the film while analyzing a sinusoidal fluted tube, but later found that two-dimensional conduction is important within the fin and the film for a triangular fin[16]. A recent analysis by Barnes and Rohsenow[17], based largely on Refs. 14 and 18, reports an augmentation ratio of about 15 for condensation of steam on a fluted surface, whereas most earlier studies considered condensation of a refrigerant and found much smaller augmentation ratios. With our present knowledge, it is difficult to ascertain whether this discrepancy is due to different fluids or to questionable analysis.

All theoretical analyses discussed above break up the fluted surface into basically two parts. In the portion near the crest, gravity is neglected in comparison to the surface tension effect, whereas in the portion near the trough, the reverse is true. The two regions are patched at a point that is selected quite arbitrarily at times[13-16]. This isolation of the two important effects is justified on the basis that the condensate film is thick in the trough region and thin over the crest. This, however, is not true over the initial portion of the tube length.

A recent analysis by Stack and Merkle[19] does attempt to solve the complete equation with both gravitational and surface tension effects included over the entire flute, but it has two major drawbacks. First, their analysis is restricted to impracticably low values (0.02 and 0.04) of amplitude-to-pitch ratio of the flute, owing to the use of a cartesian coordinate system rather than a surface-oriented coordinate system. Second, their analysis does not consider any heat transfer effects. Fujii and

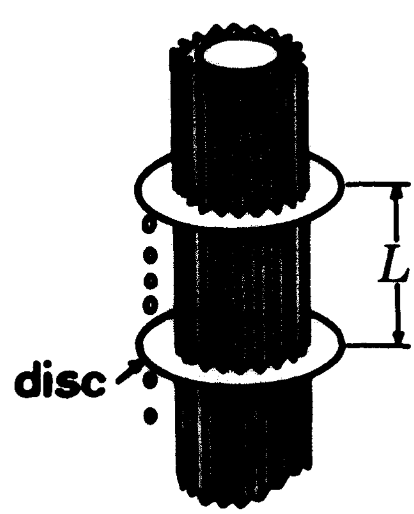

Figure 1 Vertical fluted tube

* Present address: Department of Mechanical Engineering, Ohio State University, Columbus, Ohio 43210, USA

Honda[11] also considered the entire thin film as one piece over an initial length of the tube (only about one-eighth of the flute pitch), but neglected the important surface tension effect.

A major deficiency of all the above theoretical analyses is the way the surface tension effect is determined. This effect depends not upon the curvature of the condensate-vapor interface but upon the variation of this curvature along the interface. However, since the location of this interface is unknown a priori, some analyses[10,11] simply determine it on the basis of the known flute shape. Such analyses cannot be applied at all to triangular or rectangular fins because their curvature, as well as the variation of curvature along the flute, is zero. This is not true, however, for the condensate-vapor interface. Even for sinusoidal flutes, there are large differences between the curvature and its variation along the curved surface for the given flute and the actual interface, as we show later. Moreover, the claims that these analyses determine the surface tension effect based on the shape of the condensate-vapor interface are questionable, as we show in the Appendix.

Another problem with all earlier theoretical analyses except Ref. 11 is that conduction within the condensate film and the tube wall is either completely neglected or considered to be at most one-dimensional. Panchal and Bell[16] point out clearly that two-dimensional conduction should be considered within the condensate film and the tube wall.

The analysis in this paper attempts to remove these deficiencies and presents a finite difference solution of the highly nonlinear partial differential equation for the condensate film thickness coupled with a finite element solution of the two-dimensional conduction problem.

Notation

A, B, C	Coefficients of Equation 19 as defined in Equations 20
D_1, D_2	Coefficients in Equation 15
D_3	The ratio δ_r/x_p
E_1, E_3	Dimensionless shear stresses, defined following Equations 16
F	Dimensionless derivative of radius of curvature of the condensate-vapor interface
$f(x)$	Function describing the flute shape
$f_i(x)$	Function describing the condensate-vapor interface
G	The ratio Q/Δ
g	Acceleration due to gravity
h_{fg}	Latent heat of vaporization
h_0	Half-amplitude of the flute (Figure 2)
h_t	Mean height of the flute (Figure 2)
k	Thermal conductivity
k_f	Thermal conductivity of the fluid
k_w	Thermal conductivity of the fluted tube material
L	Length of the fluted tube in the vertical direction
$\mathbf{n}_w$	Unit normal to the flute
P	Pitch of the flute
p	Pressure
p_s	Saturation pressure of the vapor
Q	Dimensionless function of the radius of curvature of the flute, defined following Equations 16
R	Radius of curvature of the fluted tube; also, right side of Equation 19 as defined in Equations 20
R_c	The ratio R/x_p
R_i	Radius of curvature of the condensate-vapor interface; also, as defined in Equation 20d
R_n	The ratio R_i/x_p; also as defined in Equation 20h
$\mathbf{r}_i$	Position vector to a point on the condensate-vapor interface
$\mathbf{r}_w$	Position vector to a point on the flute surface
S_1, S_3	Shear stresses in x_1- and z-directions, respectively
T	Temperature
T_c	Temperature at the coolant-tube interface
T_s	Saturation temperature at the condensate-vapor interface
T_w	Wall temperature
T_{w00}	Wall temperature at the initial station z_0
u_1, u_2, w	Velocity components in x_1-, x_2-, and z-directions, respectively
X	Dimensionless distance along the flute
x_1, x_2	Coordinates along and normal to the flute, respectively
x_i	Coordinate along the condensate-vapor interface
x_p	Length of curve DE along the flute (Figure 2)
x, y	Coordinates as shown in Figure 2
Z, z	Dimensionless and dimensional vertical coordinates, respectively
Z_0, z_0	Dimensionless and dimensional locations of initial station in vertical direction, respectively
α_1 to α_4	Coefficients in Equation A4
β	Parameter depending upon the finite differencing used (Equation 17)
β_1 to β_4	Coefficients in Equation A4
γ_1 to γ_8	Coefficients in Equation A6
Δ, δ	Dimensionless and dimensional condensate film thicknesses, respectively
δ_0	Condensate film thickness at the initial station z_0
δ_r	Characteristic film thickness based upon the Nusselt relation
$\delta X, \delta Z$	Step sizes in the X- and Z-directions, respectively
ε	Small number for termination of iterations
λ	Relaxation factor
μ	Dynamic viscosity of the condensate
ρ	Density of the condensate
ρ_v	Density of the vapor
σ	Surface tension

Subscripts

i, k	Represent locations in X- and Z-directions, respectively

Superscripts

m	Value at the current iteration
$'$	Derivative with respect to x or x_1

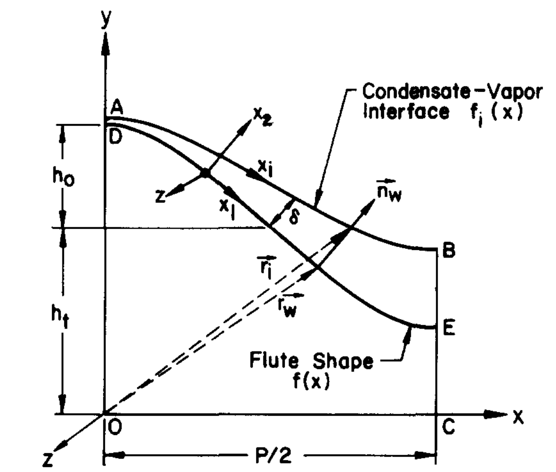

Figure 2 Coordinate system

Analysis

Consider the condensate as a viscous, incompressible Newtonian fluid, and set up a curvilinear orthogonal coordinate system (x_1, x_2, z) as shown in Figure 2. The momentum equations (Ref. 20, p. 68), simplified with the assumptions that inertia terms are negligible compared to other terms, and that $\partial/\partial x_2 \gg \partial/\partial x_1$ or $\partial/\partial z$, and $u_2 \ll u_1$ or w, then yield

$$\frac{\partial^2 u_1}{\partial x_2^2}=\frac{1}{\mu}\frac{R}{R+x_2}\frac{\partial p}{\partial x_1} \tag{1}$$

$$\frac{\partial p}{\partial x_2}=0 \tag{2}$$

$$\frac{\partial^2 w}{\partial x_2^2}=-\frac{g}{\mu}(\rho-\rho_v) \tag{3}$$

where u_1, u_2, and w are the velocity components in the x_1-, x_2-, and z-directions, respectively, $R(x_1)$ is the radius of curvature of the fluted tube, p is the pressure in the condensate film, g is the acceleration due to gravity, ρ and μ are the density and dynamic viscosity of the condensate, and ρ_v is the density of the vapor.

Integration of Equation 1 with boundary conditions

$$u_1=0 \quad \text{at } x_2=0$$

$$\mu\frac{\partial u_1}{\partial x_2}=S_1 \quad \text{at } x_2=\delta \tag{4}$$

yields

$$u_1=\frac{S_1}{\mu}x_2+\frac{R}{\mu}\frac{\mathrm{d}p}{\mathrm{d}x_1}\left[x_2\ln\left(\frac{R+x_2}{R+\delta}\right)+R\ln\left(\frac{R+x_2}{R}\right)-x_2\right] \tag{5}$$

Here S_1 is the (known) shear stress in the x_1-direction on the condensate-vapor interface, and $\delta(x_1, z)$ is the condensate film thickness. Similarly, integration of Equation 3 with boundary conditions

$$w=0 \quad \text{at } x_2=0 \tag{6}$$

$$\mu\frac{\partial w}{\partial x_2}=S_3 \quad \text{at } x_2=\delta$$

yields

$$w=\frac{S_3}{\mu}x_2+\frac{g}{\mu}(\rho-\rho_v)x_2\left(\delta-\frac{x_2}{2}\right) \tag{7}$$

Here S_3 is the (known) shear stress in the z-direction on the condensate-vapor interface.

Considering a control volume that extends over the condensate film thickness, we can write the continuity equation in integral form as

$$\frac{\partial}{\partial x_1}\int_0^\delta u_1\,\mathrm{d}x_2+\frac{\partial}{\partial z}\int_0^\delta w\,\mathrm{d}x_2=\frac{k_f}{\rho h_{fg}}\left(\frac{\partial T}{\partial x_2}\right)_{x_2=\delta} \tag{8}$$

where k_f is the thermal conductivity of the fluid, and h_{fg} is the latent heat of vaporization. The right side of Equation 8 represents the rate of condensation of vapor.

Substituting for u_1 and w from Equations 5 and 7 into Equation 8 and integrating, we get

$$\frac{S_1}{2\mu}\frac{\partial\delta^2}{\partial x_1}+\frac{\delta^2}{2\mu}\frac{\partial S_1}{\partial x_1} -\frac{1}{\mu}\frac{\partial}{\partial x_1}\left[R\frac{\mathrm{d}p}{\mathrm{d}x_1}\left\{\frac{R\delta}{2}+\frac{3\delta^2}{4}-\left(R\delta+\frac{R^2}{2}\right)\ln\left(1+\frac{\delta}{R}\right)\right\}\right] +\frac{S_3}{2\mu}\frac{\partial\delta^2}{\partial z}+\frac{\delta^2}{2\mu}\frac{\partial S_3}{\partial z}+\frac{g}{3\mu}(\rho-\rho_v)\frac{\partial\delta^3}{\partial z}=\frac{k_f}{\rho h_{fg}}\frac{T_s-T_w}{\delta} \tag{9}$$

where T_s is the saturation temperature at which condensation takes place and $T_w(x_1, z)$ is the wall temperature at $x_2=0$. The pressure p can be related to the surface tension σ and radius of curvature R_i of the condensate-vapor interface by

$$p=p_s\pm\sigma/R_i \tag{10}$$

where p_s is the saturation pressure of the vapor. The positive sign holds for $0\leqslant x_1<x_p/2$, and the negative sign for $x_p/2\leqslant x_1\leqslant x_p$, where x_p is the length of curve DE in Figure 2. We are basically interested in analyzing flute shapes that are symmetric about the crest and trough, so we consider only half of the flute pitch.

If we assume σ to be constant, Equation 10 yields

$$\frac{\mathrm{d}p}{\mathrm{d}x_1}=\pm\sigma\frac{\mathrm{d}}{\mathrm{d}x_1}\left(\frac{1}{R_i}\right) \tag{11}$$

It is thus the variation of curvature of the condensate-vapor interface, not the curvature itself, that is significant. In general, this can be quite different from $\mathrm{d}(1/R)/\mathrm{d}x_1$, a fact neglected by many previous analyses. Relations for finding $\mathrm{d}(1/R_i)/\mathrm{d}x_1$ are given in the Appendix.

Equation 9 is a partial differential equation for the condensate film thickness $\delta(x_1, z)$. It requires prior knowledge of shear stresses S_1 and S_3 that come from vapor dynamics, and of $T_w(x_1, z)$ that comes from the heat transfer analysis of the fluted tube and condensate film. This equation involves only first-order derivatives with respect to z but fourth-order derivatives with respect to x_1, owing to the presence of $\mathrm{d}p/\mathrm{d}x_1$ (cf. Equations 11 and A5). For flute shapes that are symmetric about the crest and trough, the boundary conditions for the solution of Equation 9 are

$$\frac{\partial\delta}{\partial x_1}=\frac{\partial^3\delta}{\partial x_1^3}=0 \quad \text{at } x_1=0 \text{ and at } x_1=x_p \text{ for all } z \tag{12a}$$

$$\delta(x_1, 0)=0 \tag{12b}$$

The initial condition at $z=0$ is correct, but it is not practical to start the integration of Equation 9 from $z=0$. Therefore, following Stack and Merkle[19], we replace the initial condition at $z=0$ (Equation 12b) by

$$\delta(x_1, z_0)=\delta_0 \tag{12c}$$

where δ_0, the film thickness at the initial station z_0, is determined by the classical Nusselt solution

$$\delta_0=\left\{\frac{4\mu k_f z_0(T_s-T_{woo})}{\rho(\rho-\rho_v)gh_{fg}}\right\}^{1/4} \tag{13}$$

Here $T_{woo}=T_w(0,z_0)\simeq T_w(0,0)$.

For nondimensionalization, we take the length L of the vertical fluted tube in the z-direction, and the lengths x_p and δ_r as the characteristic lengths in the x_1- and x_2-directions, respectively. Here δ_r is related to L by the Nusselt relation (equation 13) in exactly the same manner as δ_0 is related to z_0. Thus, we let

$$\Delta=\delta/\delta_r,\quad X=x_1/x_p,\quad Z=z/L \tag{14}$$

With this nondimensionalization, Equation 9 and the boundary conditions expressed by Equations 12a and 12c can be written as

$$\frac{\partial\Delta^3}{\partial Z}+D_1\frac{\partial Q}{\partial X}+E_1\frac{\partial\Delta^2}{\partial X}+E_3\frac{\partial\Delta^2}{\partial Z}+\Delta^2\left(\frac{\partial E_1}{\partial X}+\frac{\partial E_3}{\partial Z}\right)=\frac{3D_2}{4\Delta} \tag{15}$$

$$\frac{\partial\Delta}{\partial X}=\frac{\partial^3\Delta}{\partial X^3}=0 \quad \text{at } X=0,\ 1 \text{ for all } Z \tag{16a}$$

$$\Delta(X,Z_0)=Z_0^{1/4} \tag{16b}$$

where

$$Z_0=\frac{z_0}{L},\quad D_1=\frac{3\sigma L}{g(\rho-\rho_v)x_p\delta_r^2},\quad D_2=\frac{T_s-T_w}{T_s-T_{woo}}$$

$$E_1=\frac{3LS_1}{2g(\rho-\rho_v)x_p\delta_r},\quad E_3=\frac{3S_3}{2g(\rho-\rho_v)\delta_r}$$

$$Q=R_c\left[\frac{R_c\Delta}{2}+\frac{3D_3\Delta^2}{4}-\left(R_c\Delta+\frac{R_c^2}{2D_3}\right)\ln\left(1+\frac{D_3\Delta}{R_c}\right)\right]F$$

$$D_3=\frac{\delta_r}{x_p},\qquad R_c=\frac{R}{x_p}$$

$$F=\pm\frac{d}{dx}\left(\frac{1}{R_n}\right)=\pm x_p^2\frac{d}{dx_1}\left(\frac{1}{R_i}\right)$$

$$(-\text{ for } 0\leqslant X<1/2;\ +\text{ for } 1/2<X\leqslant 1)$$

$$R_n=\frac{R_i}{x_p}$$

Equation 15 is a highly nonlinear partial differential equation. It is solved numerically by the finite difference technique as detailed below.

Finite difference method

Equation 15 is parabolic in Z so that a forward marching scheme in the Z-direction can be used. Thus the choice of δ_0 will affect only the region near z_0, and its effect will die out as z increases. This was indeed found to be true. Equation 15 as written is in conservative form. An equivalent, but non-conservative, form can be obtained by expanding the derivatives in Equation 15 and dividing by $3\Delta^2$. In that nonconservative form, the equation is still parabolic in Z, but the mass is *not* identically conserved when the equation is integrated numerically[19].

We divide the interval $0\leqslant X\leqslant 1$ into n equal parts. Taking δX and δZ as the step sizes in the X- and Z-directions, respectively, and using backward differencing in the Z-direction and mixed differencing in the X-direction, we can write the finite difference form of Equation 15 as

$$\frac{\Delta_{i,k}^3-\Delta_{i,k-1}^3}{\delta Z}+D_1\frac{\beta Q_{i+1,k}+(1-2\beta)Q_{i,k}-(1-\beta)Q_{i-1,k}}{\delta X}$$
$$+E_1\frac{\beta\Delta_{i+1,k}^2+(1-2\beta)\Delta_{i,k}^2-(1-\beta)\Delta_{i-1,k}^2}{\delta X}+E_3\frac{\Delta_{i,k}^2-\Delta_{i,k-1}^2}{\delta Z}$$
$$+\Delta_{i,k}^2\left(\frac{\partial E_1}{\partial X}+\frac{\partial E_3}{\partial Z}\right)_{i,k}=\frac{3D_2}{4\Delta_{i,k}} \tag{17}$$

where the subscripts i and k represent the locations in the X- and Z-directions, respectively, and β is a parameter between 0 and 1. $\beta=0$ corresponds to backward differencing, $\beta=1$ to forward differencing, and $\beta=\frac{1}{2}$ to central differencing in X. Since Equation 16b gives Δ's for all X (i.e., for all $i=0(1)n$) at Z_0 (say $k=1$), we can march forward in the Z-direction.

Equation 17 leads to a tridiagonal set of nonlinear algebraic equations to be solved for $n+1$ values of Δ's at each location k of forward march in the Z-direction. This nonlinear set is solved by linearization and successive iteration. Three methods were used for linearization, and their details are presented in Ref. 21. Of these, the one that worked best uses a Taylor series expansion to linearize terms containing Δ^2 and Δ^3. Thus we let

$$(\Delta_{i,k}^3)^m=3(\Delta_{i,k}^2)^{m-1}(\Delta_{i,k})^m-2(\Delta_{i,k}^3)^{m-1} \tag{18a}$$

and

$$(\Delta_{i,k}^2)^m=2(\Delta_{i,k})^{m-1}(\Delta_{i,k})^m-(\Delta_{i,k}^2)^{m-1} \tag{18b}$$

where $(\ )^m$ and $(\ )^{m-1}$ represent the values at the (current) mth and (previous) $(m-1)$th iteration, respectively. With this linearization, Equation 17 can be written as

$$A_i(\Delta_{i-1,k})^m+B_i(\Delta_{i,k})^m+C_i(\Delta_{i+1,k})^m=R_i \tag{19}$$

where the coefficients are

$$A_i=-\frac{\delta Z}{\delta X}(1-\beta)[D_1(G_{i-1,k})^{m-1}+2E_1(\Delta_{i-1,k})^{m-1}],\qquad i=1,2,\ldots,n-1 \tag{20a}$$

$$B_i=(\Delta_{i,k})^{m-1}\left[3(\Delta_{i,k})^{m-1}+2E_3+2\delta Z\left(\frac{\partial E_1}{\partial X}+\frac{\partial E_3}{\partial Z}\right)_{i,k}\right]$$
$$+\frac{\delta Z}{\delta X}(1-2\beta)[D_1(G_{i,k})^{m-1}+2E_1(\Delta_{i,k})^{m-1}],\qquad i=0,1,\ldots,n \tag{20b}$$

$$C_i=\frac{\delta Z}{\delta X}\beta[D_1(G_{i+1,k})^{m-1}+2E_1(\Delta_{i+1,k})^{m-1}],\qquad i=1,2,\ldots,n-1 \tag{20c}$$

$$R_i=\Delta_{i,k-1}^3+E_3\Delta_{i,k-1}^2+\frac{3D_2\delta Z}{4(\Delta_{i,k})^{m-1}}+2(\Delta_{i,k}^3)^{m-1}$$
$$+E_1\frac{\delta Z}{\delta X}[\beta(\Delta_{i+1,k}^2)^{m-1}+(1-2\beta)(\Delta_{i,k}^2)^{m-1}-(1-\beta)(\Delta_{i-1,k}^2)^{m-1}]$$
$$+\left[E_3+\delta Z\left(\frac{\partial E_1}{\partial X}+\frac{\partial E_3}{\partial Z}\right)_{i,k}\right](\Delta_{i,k}^2)^{m-1},\qquad i=1,2,\ldots,n-1 \tag{20d}$$

$$A_n=-\frac{\delta Z}{\delta X}[D_1(G_{n-1,k})^{m-1}+2E_1(1-2\beta)(\Delta_{n-1,k})^{m-1}] \tag{20e}$$

$$C_0=\frac{\delta Z}{\delta X}[D_1(G_{1,k})^{m-1}-2E_1(1-2\beta)(\Delta_{1,k})^{m-1}] \tag{20f}$$

$$R_0=\Delta_{0,k-1}^3+E_3\Delta_{0,k-1}^2+\frac{3D_2\delta Z}{4(\Delta_{0,k})^{m-1}}-E_1\frac{\delta Z}{\delta X}(1-2\beta)(\Delta_{1,k}^2)^{m-1}$$
$$+(\Delta_{0,k}^2)^{m-1}\left[2(\Delta_{0,k})^{m-1}+E_1\frac{\delta Z}{\delta X}(1-2\beta)+E_3+\delta Z\left(\frac{\partial E_1}{\partial X}+\frac{\partial E_3}{\partial Z}\right)_{0,k}\right] \tag{20g}$$

$$R_n=\Delta_{n,k-1}^3+E_3\Delta_{n,k-1}^2+\frac{3D_2\delta Z}{4(\Delta_{n,k})^{m-1}}-E_1\frac{\delta Z}{\delta X}(1-2\beta)(\Delta_{n-1,k}^2)^{m-1}$$
$$+(\Delta_{n,k}^2)^{m-1}\left[2(\Delta_{n,k})^{m-1}+E_1\frac{\delta Z}{\delta X}(1-2\beta)+E_3+\delta Z\left(\frac{\partial E_1}{\partial X}+\frac{\partial E_3}{\partial Z}\right)_{n,k}\right] \tag{20h}$$

and where $G=Q/\Delta$ and the boundary conditions in Equation 16a have been accounted for.

For successive iterations to converge, it is also necessary to underrelax the values of Δ after every iteration according to the FORTRAN statement

$$(\Delta)^m=(\Delta)^{m-1}+\lambda[(\Delta)^m-(\Delta)^{m-1}] \tag{21}$$

where the relaxation factor $\lambda<1$.

Note from Equations 20 that the Taylor series expansion was *not* used to linearize the right side of Equation 17 or the terms involving Q on the left side of Equation 17. Although such a linearization of the right side of Equation 17 was not found to be beneficial, that of the terms involving Q in Equation 17 was found not to work at all. Additional details of this situation are given in Ref. 21.

Computational details

Before the set of Equations 19 resulting from Equation 17 can be solved, we need to specify values of the dimensionless parameters E_1, E_3, and D_2. This requires prior knowledge of the shear stresses S_1 and S_3 and the temperature $T_w(x_1,z)$ of the condensate-wall interface. The computer code does have a provision for specifying S_1 and S_3, but for the present results both these stresses were set to zero. The computer code, however, does calculate $T_w(x_1,z)$ by considering two-dimensional conduction within the fluted tube wall as well as within the condensate film. For this, the Laplace equation

$$k\left(\frac{\partial^2 T}{\partial x^2}+\frac{\partial^2 T}{\partial y^2}\right)=0 \tag{22}$$

is solved subject to the boundary conditions

$$\frac{\partial T}{\partial x}=0 \quad \text{at } x=0,\ P/2 \tag{23}$$

where P = pitch of the flute
$T=T_s$ at the condensate-vapor interface
$T=T_c$ at the coolant-tube interface

and k is the thermal conductivity, and T_c is the coolant temperature, which is assumed to vary linearly from the coolant inlet to exit temperature.

The solution to the system 22 and 23 was obtained by a finite element method in which region $OABCO$ (Figure 2) was divided into several linear triangular elements. Details can be found in any text on the finite element method, but some care is required since the thermal conductivity of the fluid in region $ABEDA$ is vastly different from that of the tube material in region $DECOD$ (Figure 2). This solution yields the values of $T_w(x_1,z)$ on the surface DE (Figure 2).

It is therefore obvious that the solutions of Equations 17 and 22 are coupled. Also, since the solution of Equation 17 is found iteratively, Equation 22 should also be solved at every iteration. This places a rather prohibitive demand on computer time. However, since δZ is small (about 10^{-5}), changes in δ are small at every iteration, with the result that Equation 22 can be solved only once per step in the Z-direction. This saves considerable computer time at the cost of really negligible error in δ and heat transfer values, as confirmed by some initial runs.

Successful solution of Equation 17 requires the correct calculation of the highly nonlinear parameter Q, which involves the computation of $d(1/R_i)/dx_1$. An equation for the evaluation of this derivative is given in the Appendix, and additional details can be found elsewhere[21]. Use of Equation A5 to find this derivative requires the determination of the first three derivatives of δ with respect to x_1. Though δ is known at equidistant values of x_1, numerical calculation of higher-order derivatives is always problematic due to amplification of noise in the data. Several methods were therefore tried with varying degrees of success[21]. Of these, the best method turned out to be the use of central difference relations.

Results and discussion

Results are presented for one vapor-tube combination for which experimental data is also available. Specifically, results were computed for tube F of Refs. 8 and 9. This tube was made of aluminum, was smooth on the inside, and had 48 external flutes. It had an internal diameter of 22.9 mm and an overall condensing length of 1.168 m. Data were available for condensation of several refrigerants on its outer surface[9]. However, the particular case chosen for comparison was for condensation of freon-113 on the tube while it was covered with seven rubber condensate drainage skirts equally spaced along its vertical axis. These skirts were designed to strip the condensate away from the tube wall, thereby providing eight equally spaced condensation lengths of 142.875 mm each. Details of the actual shape of the flute and its dimensions are not available in Refs. 8 and 9, so they were approximated from an enlarged photograph contained in Ref. 9. The relevant fluid and tube properties used in the analysis are

$\rho=1498$ kg/m^3	$\rho_v=8.586$ kg/m^3
$\mu=4.8\times10^{-4}$ kg/m-s	$\sigma=0.0143$ N/m
$h_{fg}=145.23$ kJ/kg	$k_f=0.07$ W/m-K
$k_w=205$ W/m-K	$T_s=325.5$ K
$T_{woo}=318.5$ K	$T_c=318.5$ K(in), 318.8 K(out)
$L=142.875$ mm	$P=1.614$ mm
$h_t=0.881$ mm	$h_0=0.1554$ mm

where k_w is the thermal conductivity of the fluted tube material and h_t and h_0 are associated with the flute shape (Figure 2), taken to be

$$f(x)=h_t+h_0\cos\left(\frac{2\pi x}{P}\right) \tag{24}$$

The amplitude-to-pitch ratio of this flute is ~0.2.

After some numerical experimentation involving different step sizes, etc., the solution of Equation 17 was started from $Z_0=5\times10^{-6}$ with $\beta=\frac{1}{2}$, $\delta X=0.05$, an initial $\delta Z=5\times10^{-6}$, and an initial $\lambda=0.5$. Further iteration for the solution of

Equation 17 was terminated when

$$|1-(\Delta_{i,k})^{m-1}/(\Delta_{i,k})^{m}|<\varepsilon \quad \text{for all } i \text{ at every } k \tag{25}$$

where ε was taken to be 10^{-6}. As the solution marched downstream in the Z-direction, δZ was increased and the relaxation factor λ had to be decreased according to Table 1, which also gives an idea of the number of iterations required before Equation 25 was satisfied.

Table 1 Some parameters for solving Equation 17

δZ	λ		Z	No. of iterations
5×10^{-6}	0.5	up to	0.002	~15
8×10^{-6}	0.2	up to	0.01	~30
1.25×10^{-5}	0.1	up to	0.0225	~50
2×10^{-5}	0.06	up to	0.086	~90

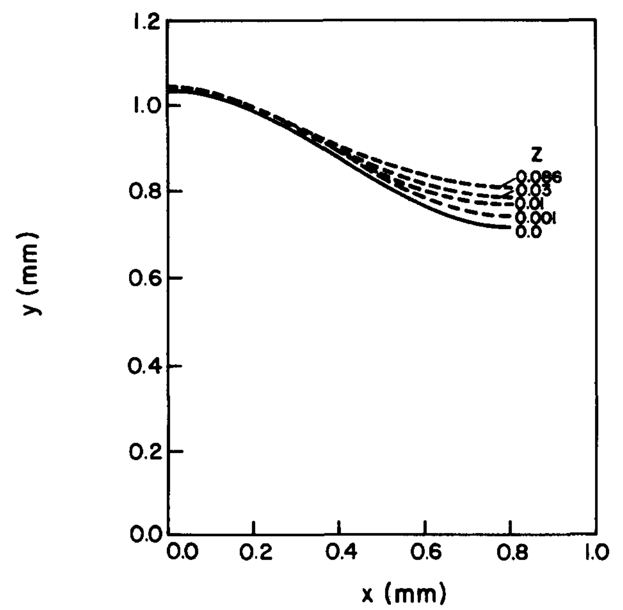

Figure 3 Fluted shape (——) and correct film shapes at some Z locations

Three different divisions of the region $OABCO$ (Figure 2) into finite elements for the solution of Equation 22 were tried. The one selected on the basis of adequate computational accuracy and relatively economical calculation had 154 triangular elements with 108 nodes. There were 11 nodes each on faces AB, BC, OC, and DE (Figure 2), and 15 nodes on face AO.

Figure 3 shows to true scale the flute shape (solid curve) and the condensate film shapes (dashed curves) at $Z=0.001$, 0.01, 0.03, and 0.086. As expected, the film thickens quite rapidly in the trough region while remaining thin over the crest. Unfortunately, it was not possible to obtain any results for Z much greater than 0.086, because convergence of the solution for the film thickness (for the same tolerance ε) became very slow. The principal reason for this slow convergence was the thickening of the film in the trough. It is clear from Figure 4, which shows the absolute value of $d(1/R_i)/dx_1$ at various Z-values, that this derivative becomes negligible in the trough region as compared to its value in the crest region. It is therefore appropriate to neglect surface tension effects in the trough region *once* the condensate film has thickened. Figure 4 also plots the absolute value of the derivative of flute curvature ($Z=0$) with respect to x_1, and even at the low value of $Z=0.002$ it is very different from the derivative of the condensate-vapor-interface curvature. This clearly brings out the error in those analyses that determine the surface tension effect on the basis of the known flute shape.

An extension of this work to $Z>0.086$, with the above considerations, is underway. It is encouraging to note from Figure 5 that a linear extrapolation, on a log-log basis, of the results to date to $Z=1$ compare well with the experimental data. Figure 5 shows the heat load (in watts) per half flute as a function of Z. This relationship is linear on a log-log basis. The solid portion of the straight line is based on the computed results of this analysis, and the dashed portion is the extrapolation. The circled point is based upon experimental data[9]. As part of this analysis, the heat transfer rates across faces AB and OC in Figure 2 were compared, and agreement was within 1%. Under steady-state conditions, of course, they should theoretically be identical, since faces OA and BC are insulated.

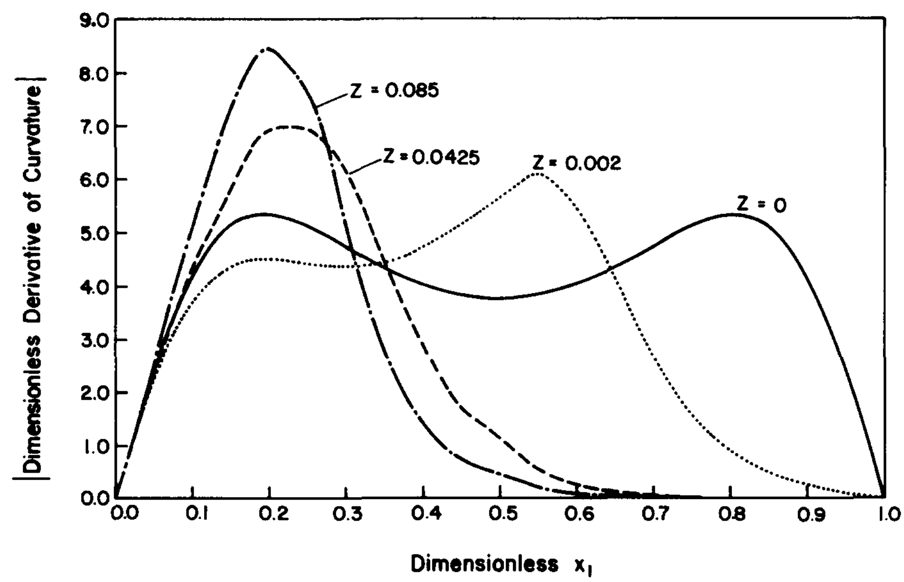

Figure 4 Comparison of dimensionless derivative of the curvature of flute (——) and condensate-vapor interface at various Z locations

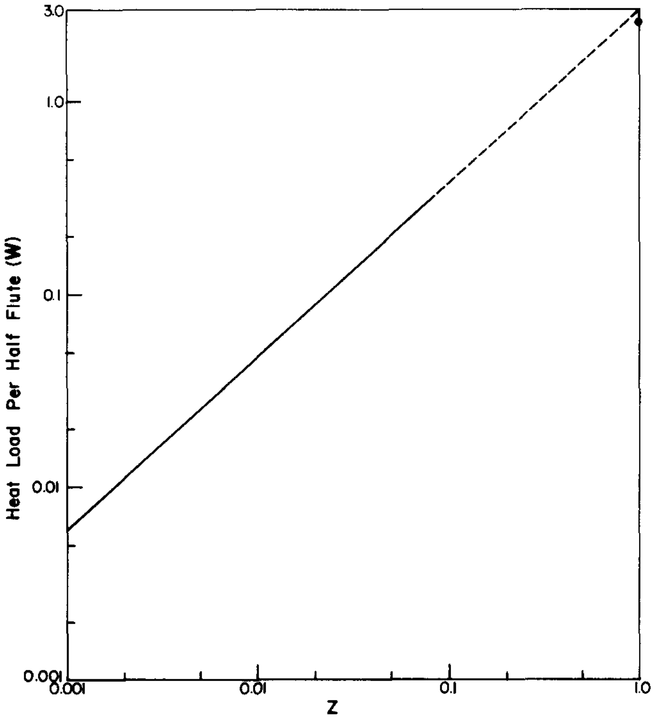

Figure 5 Heat load (in watts) as a function of Z: ——, computed; – – –, extrapolated; ●, experimental[9]

Conclusions and recommendations

Besides a critical review of the existing literature on film condensation on vertical fluted tubes, a successful attempt has been made to correctly account for both surface tension and gravitational effects over the entire flute shape in the initial portion of the tube height. This is done by use of a surface-oriented coordinate system so as to be able to analyze flute shapes with practical values of amplitude-to-pitch ratio. Two-dimensional conduction within the condensate film and the fluted tube wall is also considered.

Besides the deficiencies mentioned above, an assumption common to all previous analyses, and far more serious in terms of correctly modeling practical applications, is the complete neglect of vapor shear on the interface. The present analysis does have the provision for studying this effect, but to date the vapor shear has been taken to be zero. One should also consider the coolant dynamics to obtain a complete solution, but all this will undoubtedly be very demanding.

Acknowledgments

This research was supported in part by the Naval Postgraduate School Foundation Research Program. The first author would also like to acknowledge support by National Science Foundation Grant MCS82-01340.

References

1 Williams, A. G., Nandapurkar, S. S., and Holland, F. A. A review of methods for enhancing heat transfer rate in surface condensers. *Chem. Engr. Lond.* 1968, CE367–CE373
2 Gregorig, R. Hautkondensation an Feingewellten Oberflachen Bei Berucksichtigung der Oberflachen-spannungen. *Z. Angew. Math. Phys.* 1954, 36–49
3 Lustenader, E. L., Richter, R., and Neugebauer, F. J. The use of thin films for increasing evaporation and condensation rates in process equipment. *J. Heat Transfer, Trans. ASME* 1959, **81**, 297–307
4 Carnavos, T. C. Thin-film distillation. Proc. First Int. Symp. on Water Desalination, Paper SWD-17, Washington, 1965
5 Thomas, D. G. Enhancement of film condensation heat transfer rates on vertical tubes by vertical wires. *Ind. Eng. Chem. Fund.* 1967, **6**, 97–103
6 Thomas, D. G. Enhancement of film condensation rate on vertical tubes by longitudinal fins. *AIChE J.* 1968, **14**, 644–649
7 Newson, I. H. and Hodgson, T. D. The development of enhanced heat transfer condenser tubing. *Desalination* 1974, **14**, 291–323
8 Combs, S. K. Experimental data for ammonia condensation on vertical and inclined fluted tubes. Report ORNL-5488, 1979
9 Combs, S. K., Mailen, G. S., and Murphy, R. W. Condensation of refrigerants on vertical fluted tubes. Report ORNL/TM-5848, 1978
10 Edwards, D. K., Gier, K. D., Ayyaswamy, P. S., and Catton, I. Evaporation and condensation in circumferential grooves on horizontal tubes, ASME paper 73-HT-25, 1973
11 Fujii, T. and Honda, H. Laminar filmwise condensation on a vertical single fluted plate. Proc. Sixth Int. Heat Transfer Conf., Toronto, Vol. 2, 1978, pp. 419–424
12 Mori, Y., Hijikata, K., Hirasawa, S., and Nakayama, W. Optimized performance of condensers with outside condensing surfaces. *J. Heat Transfer, Trans. ASME* 1981, **103**, 96–102
13 Hirasawa, S., Hijikata, K., Mori, Y., and Nakayama, W. Effect of surface tension on condensate motion in laminar film condensation (study of liquid film in a small trough). *Int. J. Heat Mass Transfer* 1980, **23**, 1471–1478
14 Panchal, C. B. and Bell, K. J. Analysis of Nusselt-type condensation on a vertical fluted surface. In *Condensation Heat Transfer*, eds. P. J. Marto and P. G. Kroeger, ASME, 1979, pp. 45–53
15 Panchal, C. B. and Bell, K. J. Analysis of Nusselt-type condensation on a vertical fluted surface. *Num. Heat Transfer* 1980, **3**, 357–371
16 Panchal, C. B. and Bell, K. J. Analysis of Nusselt-type condensation on a triangular fluted surface. *Int. J. Heat Mass Transfer* 1982, **25**, 1909–1911
17 Barnes, C. G. Jr., and Rohsenow, W. M. Vertical fluted tube condenser performance prediction. Proc. 7th Int. Heat Transfer Conf. Munich, 5, 1982, pp. 39–43
18 Yamamoto, H. and Ishibachi, T. Calculation of condensation heat transfer coefficients of fluted tubes. *Heat Transfer Japanese Res.* 1977, **6**, 61–69
19 Stack, T. G. and Merkle, C. L. Laminar filmwise condensation on a fluted vertical surface. Manuscript submitted to *Int. J. Heat Mass Transfer*, 1983.
20 Schlichting, H. *Boundary Layer Theory*, 7th ed. McGraw-Hill, 1979
21 Garg, V. K. and Marto, P. J. Heat transfer due to film condensation on vertical fluted tubes. NPS Report No. NPS 69-84-006, Naval Postgraduate School, 1984

Appendix: Condensate-vapor-interface curvature

Let $f(x)$ denote the flute shape (Figure 2), and $\mathbf{r}_w$ and $\mathbf{r}_i$ be the position vectors to points on the flute and condensate-vapor interface, respectively. Then

$$\mathbf{r}_i - \mathbf{r}_w = \mathbf{n}_w \delta \tag{A1}$$

where $\mathbf{n}_w$ is the unit normal to the flute, given by

$$\mathbf{n}_w = (1 + f'^2)^{-1/2}(-f', 1) \tag{A2}$$

where $f' = df/dx$. If we let x_i be the curvilinear coordinate along the condensate-vapor interface, we have by definition

$$\frac{1}{R_i} \equiv \left|\frac{\partial^2 \mathbf{r}_i}{\partial x_i^2}\right| = \left|\frac{\partial^2(\mathbf{r}_w + \mathbf{n}_w \delta)}{\partial x_i^2}\right| \simeq \left|\frac{\partial^2 \mathbf{r}_w}{\partial x_1^2} + \delta \frac{\partial^2 \mathbf{n}_w}{\partial x_1^2} + 2\frac{\partial \mathbf{n}_w}{\partial x_1}\frac{\partial \delta}{\partial x_1} + \mathbf{n}_w \frac{\partial^2 \delta}{\partial x_1^2}\right| \tag{A3}$$

where $\partial/\partial x_i$ has been approximated by $\partial/\partial x_1$. Noting that $\mathbf{r}_w = (x, f)$, and $\mathbf{n}_w$ is given by Equation A2, we get from Equation A3, after some lengthy algebra, the relation

$$\frac{1}{R_i} = [(\alpha_1 + \alpha_2\delta + \alpha_3\delta' + \alpha_4\delta'')^2 + (\beta_1 + \beta_2\delta + \beta_3\delta' + \beta_4\delta'')^2]^{1/2} \tag{A4}$$

where $\delta' \equiv \partial\delta/\partial x_1$, etc., and

$$\alpha_1 = -\beta_1 f', \qquad \alpha_2 = (1+f'^2)^{-5/2}\left(\frac{4f'f''^2}{1+f'^2} - f'''\right)$$

$$\alpha_3 = -2\beta_1, \qquad \alpha_4 = -\beta_4 f'$$

$$\beta_1 = f''(1+f'^2)^{-2}, \qquad \beta_2 = \alpha_2 f' - \beta_1\beta_4 f''$$

$$\beta_3 = 2\alpha_1, \qquad \beta_4 = (1+f'^2)^{-1/2}$$

From Equation A4 it follows that

$$\begin{aligned}\frac{d}{dx_1}\left(\frac{1}{R_i}\right) = R_i\{&(\alpha_1 + \alpha_2\delta + \alpha_3\delta' + \alpha_4\delta'') \\ &\times(\beta_2 + \alpha_2'\delta + 3\alpha_2\delta' - 3\beta_1\delta'' + \alpha_4\delta''') \\ &+(\beta_1 + \beta_2\delta + \beta_3\delta' + \beta_4\delta'') \\ &\times(-\alpha_2 + \beta_2'\delta + 3\beta_2\delta' + 3\alpha_1\delta'' + \beta_4\delta''')\}\end{aligned} \tag{A5}$$

where

$$\alpha_2' = \frac{d\alpha_2}{dx_1} = (1+f'^2)^{-3}\left[\frac{f''(4f''^2 + 13f'f''')}{1+f'^2} - f^{iv} - \frac{28f'^2 f''^3}{(1+f'^2)^2}\right]$$

and

$$\beta_2' = \frac{d\beta_2}{dx_1} = \alpha_2' f' + f''(2\beta_4\alpha_2 - \alpha_1\beta_1) - \beta_1\beta_4^2 f'''$$

Though the relation for $d(1/R_i)/dx_1$ in Equation A5 is somewhat approximate, it was preferred over the exact relation, since the latter yields mild oscillations in values of δ upon integration of Equation 9 by a few steps in the Z-direction. Writing $\mathbf{r}_i$ as

$$\mathbf{r}_i = (x - \delta f'\beta_4, f + \delta\beta_4)$$

we can show[21] that the exact relation for the curvature of the condensate-vapor interface is

$$\frac{1}{R_i} = \frac{|\gamma_5\delta'' + \gamma_4\delta\delta' + \gamma_3\delta + \gamma_2\delta^2 + \gamma_1(1 - \delta\delta'' + 2\delta'^2)|}{[\gamma_6(1+\delta'^2) + \gamma_7\delta^2 + \gamma_8\delta]^{3/2}} \tag{A6}$$

where γ_1 to γ_8 are related[21] to derivatives of $f(x)$ with respect to x, and in particular $\gamma_5 = \gamma_6^{3/2}$. Many theoretical analyses that claim to determine the surface tension effect based upon the actual shape of the condensate-vapor interface do not actually do so, since they invariably use

$$\frac{1}{R_i} = \delta''/(1+\delta'^2)^{3/2} \tag{A7}$$

for the curvature of the interface. This follows from the exact relation (Equation A6) if only the first terms in both the numerator and the denominator are retained. However, even for small δ, there is hardly any justification for dropping all other terms in Equation A6. The difference between the actual $d(1/R_i)/dx_1$ and that obtained from Equation A7 gets further amplified due to differentiation.